Journal of Materials Chemistry C

ROYAL SOCIETY OF CHEMISTRY

PAPER

View Article Online
View Journal | View Issue

Cite this: J. Mater. Chem. C, 2021, 9, 10037

Luminescent heteroleptic Eu(III) probes for the selective detection of diethyl chlorophosphate as a G-series nerve agent mimic in the vapor phase using solid-state films†

Zafar Abbas,[a] Usha Yadav,[a] Ray J. Butcher [b] and Ashis K. Patra *[a]

The extreme toxicity of innocuous organophosphate (OP) nerve agents poses a significant public health risk. Developing an efficient sensing and detection system is crucial to contain and mitigate disasters and strengthen national security. Luminescence spectroscopy offers very sensitive, visually identifiable color changes to enable a low-cost option for the specific detection of nerve agents. Lanthanide ions exhibit unique optical properties due to sensitized f → f transitions over organic fluorophores for developing luminescent optical sensors. Here, we designed two heteroleptic time-resolved luminescent Ln(III)-probes, namely, [Eu(***o***-**HPIP**)(TTA)$_3$] ([**Eu(*o*-OH)**]) and [Eu(***p***-**HPIP**)(TTA)$_3$] ([**Eu(*p*-OH)**]), for the selective sensing of the G-series nerve agent simulant diethyl chlorophosphate (DCP). The molecular identity, speciation, and optical properties of the complexes were evaluated using various physicochemical and spectroscopic methods in solution. The solid-state structure of **Eu(*o*-OH)** shows an eight-coordinated {LnN$_2$O$_6$} square-antiprismatic geometry. The interaction of the Eu(III) probes with DCP results in selective quenching of the characteristic red luminescence of Eu(III) originating from the $^5D_0 \rightarrow {}^7F_J$ (J = 0–4) f → f transitions with a limit of detection (LOD) reaching up to the ppb level for DCP {LOD: 18 ppb [**Eu(*o*-OH)**] and 10 ppb [**Eu(*p*-OH)**]}. Selective luminescence quenching is distinctly perceptible to the naked eye under UV-illumination (λ = 365 nm). The phenyl hydroxyl group was strategically incorporated at the periphery of the HPIP ligand anticipating possible nucleophilic attack at the P–Cl bond of DCP, thereby perturbing the EnT pathway from the ligand to Eu(III). The NMR titration data and the structure of the isolated thermodynamically stable polymeric **[Eu(DHP)$_3$]$_n$** end-product formed by the reaction of **Eu(*o*-OH)** with DCP confirm chemical changes that block the indirect-energy transfer from the ***o*/*p*-HPIP/TTA** antenna to the emissive $^5D_0$ state of Eu(III) causing significant quenching of time-resolved luminescence (TRL) intensity. Vapor phase detection of OP-simulants was attempted using a Eu(III)-probe immobilized on a low-cost filter paper strip. We observed consistent emission quenching of filter paper strips upon exposure to DCP vapors. The changes in Eu(III)-TRL intensity avoid any background autofluorescence and possible photobleaching associated with organic fluorophores. These absorbent paper strips could be developed as a prototype for the selective on-site detection of G-series nerve agents.

Received 12th April 2021,
Accepted 28th June 2021

DOI: 10.1039/d1tc01685g

rsc.li/materials-c

Introduction

Human exposure to most toxic chemical warfare agents (CWAs) or nerve gases remains a critical concern for human health and national security.[1] Most of the nerve gases are odorless, colorless, tasteless, and harmful below our sensory threshold. These most nefarious chemicals have very low median lethal doses (LD_{50}) for humans. They could be used as weapons of mass destruction (WMDs) due to their easy production, transportation and vapor-phase (aerosols) deployment without much technical expertise associated with inadequate monitoring and surveillance.[2] Apparently, the featureless attributes of OP nerve

[a] Department of Chemistry, Indian Institute of Technology Kanpur, Kanpur 208016, Uttar Pradesh, India. E-mail: akpatra@iitk.ac.in
[b] Department of Chemistry, Howard University, Washington, DC 20059, USA

† Electronic supplementary information (ESI) available: Characterization of the probes (ESI-MS, FT-IR, TGA), crystallographic structure details, absorption, luminescence properties, PL responses of the Eu(III) probes with acids or bases, ^{1}H-NMR of **La(*o*-OH)** with DCP, detection limit (PDF). Crystal structure data for **Eu(*o*-OH)**, **La(*o*-OH)** and the [**Eu(DHP)$_3$**]$_n$ polymeric product (CIF file). CCDC 2049309, 2049310 and 2069827. For ESI and crystallographic data in CIF or other electronic format see DOI: 10.1039/d1tc01685g

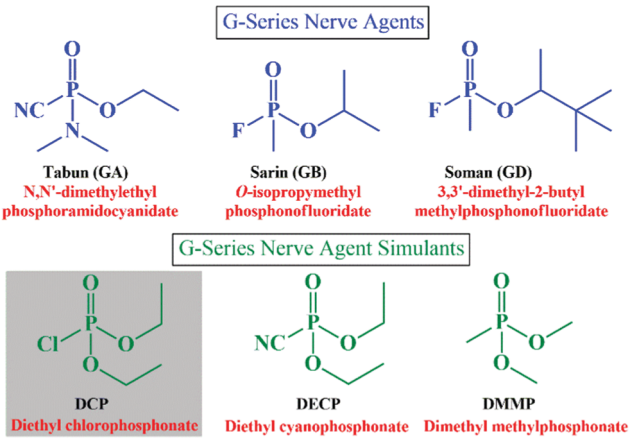

Fig. 1 Chemical structures of the G-series nerve agents and their relatively non-toxic simulants. Diethyl chlorophosphate (DCP) was selectively detected in this work.

agents make their detection even more challenging before inhalation compared to various other explosive materials or WMDs. The nerve agents are OPs of the general formulation [RO(O═P)(X)(OR′)] with X = F, CN, SR″ (Fig. 1). The substituent in P–X bond serves as a labile leaving group upon the nucleophilic phosphorylation reaction.[3,4] The nerve agents are highly reactive at the active site of cholinergic enzyme-acetylcholinesterase (AChE) that mediates the hydrolysis of the acetylcholine (ACh) neurotransmitter.[5] The kinetically and thermodynamically favorable irreversible phosphorylation reaction with the serine hydroxyl group in the esteratic site prevents binding of ACh and its subsequent hydrolysis (Scheme 1). This inhibition of AChE causes accumulation of ACh in the synapses, with continuous activated state of ACh-receptors, thereby blocking the muscle relaxation. The disruption of neurotransmission signals results in respiratory failure and neuromuscular paralysis, and immediate death.[6,7] The lethal dose (LD_{50}) for G-agents is 0.069–117.9 mg kg^{-1}, while for much more stable V-agents LD_{50} is only 0.0082–1.402 mg kg^{-1}.[8] The extreme toxicity, easy accessibility, and deployability of nerve agents make them an extreme threat to human life and national security. Therefore, reliable, easy-to-use selective sensing for rapid detection and monitoring of such lethal CWAs is of great priority and crucial for national security. Various OP derivatives are typically used as nerve agent simulants (mimics) and as target analytes in place of real nerve agents in academic research (Fig. 1). Diethyl chlorophosphate (DCP) is used as a target analyte to mimic G-series nerve agents like sarin (GB) and soman (GD).[9] Considering the threat of CWAs, several detection methods like GC-MS, ion mobility spectrometry, enzymatic activity-based, surface acoustic wave (SAW), interferometry, colorimetric and fluorogenic methods have been developed.[10–17] Monitoring of CWAs by the change in the color of colorimetric or fluorogenic probes is relatively convenient, cost-effective, and portable and sometimes offers qualitative naked eye detection in real-time.[18–23] Mostly organic chromo-fluorogenic probes are reported for such detection with a few recent examples of luminescent 4d/5d-block transition metal complexes. Emissive Ru(II) and Ir(III) complexes were recently reported for selective detection of OP nerve agent simulants and pesticides based on phosphorylation of the reactive site in the ligands by OP agents, thereby inducing modulation of color or emission intensity.[24,25] Swager and coworkers reported a hi-tech wireless wearable hazard badge based chemical dosimeter linked to the changes in chemiresistance for the remote detection of DCP.[26] Some of these organic chromo-fluorogenic probes show certain limitations, like a poor S/N ratio, background

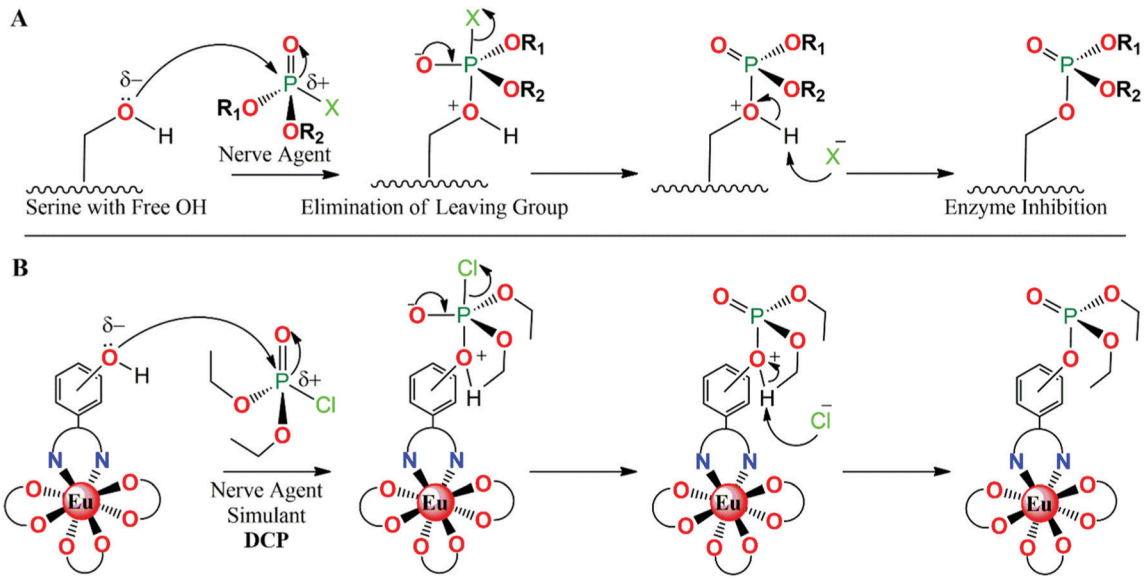

Scheme 1 (A) Nucleophilic attack of the free –OH of the serine residue at the active site of acetylcholinesterase (AChE) on the electrophilic P-atom of nerve agents, followed by removal of the leaving group (X) leading to irreversible inhibition of the enzyme active site. (B) Our design is based on a similar nucleophilic attack of the free OH group at the periphery of the probes on the P–Cl bond of the DCP nerve agent simulant, resulting in the formation of a phosphorylated product and perturbation of EnT pathways affecting Eu(III)-luminescence.

autofluorescence, photobleaching, false positive responses, *etc.* Luminescent lanthanide probes could effectively bypass these inherent limitations of organic fluorophores due to their unique excited electronic states derived from highly shielded f-orbitals.

The unique luminescence properties of lanthanides originate from intraconfigurational f → f transitions linked to their shielded inner f-orbital electrons exhibiting very well-defined electronic states unperturbed by the ligands. Luminescent Ln(III)-probes display characteristic intense sharp line-like emission spectra with high color purity ranging from the UV-vis to the NIR region. The long-lived (μs–ms) emissive excited states of Ln(III) allow highly sensitive time-delayed photoluminescence measurements to detect an analyte, thus eliminating short-lived background autofluorescence for a higher S/N ratio. Other added advantages are the large ligand-based pseudo-Stokes shift ($\lambda_{ex} - \lambda_{em}$) which enables measurements over a wide spectral window and the photobleaching resistance of Ln(III) luminescence.[27] These desirable features of emissive Ln(III) probes make them the superior choice for a specific analyte that alters the optical output by modifying the underlying energy-transfer pathways. However, the 4f → 4f transitions are electric dipole (ED) and Laporte forbidden, resulting in very weak absorptions ($\varepsilon \sim 0.1$–$10\ M^{-1}\ cm^{-1}$), and therefore the direct excitation *via* absorption of Ln(III) ions is ineffective. An energy-absorbing organic chromophore (antenna) was linked to Ln(III) ions to circumvent this limitation. The light-harvesting antenna is generally an aromatic or unsaturated organic molecule that effectively absorbs the radiation and indirectly transfers this energy non-radiatively to populate the emissive excited state (Ln*).[27] The radiative decay of Ln* to the ground state results in bright luminescence with all the characteristic features mentioned above. Designing luminescent Ln(III) probes is a multi-pronged approach based on the underlying photosensitization pathways and a subtle balance of multiple intricate radiative and non-radiative EnT pathways. Meade and coworkers extensively reviewed various design principles of analyte-responsive Ln-optical probes and their underlying hypotheses.[28] In a nutshell, the detection or sensing of a specific analyte by the antenna-conjugated sensitized luminescent Ln(III) probes is based on the perturbation of the overall energy transfer pathways and thereby alteration of various optical parameters as a measuring yardstick. Luminescent lanthanide complexes were used as OP sensors based on their competitive binding of phosphoryl oxygen (P═O) to hard oxophilic Ln(III) ions and quenching of non-radiative vibrational energy transfer. Other strategies involve phosphorylation at the coordinating site of the antenna and its concomitant displacement and deactivation of the antenna effect.[29–35]

Towards our continuous efforts to explore the lanthanide chemistry and utilizing fascinating Ln(III) luminescence for diverse interdisciplinary applications, we realized that organophosphates are a judicious and critical choice as analytes for sensing *via* time-delayed luminescence spectroscopy. Herein, our design involves two luminescent Eu(III) complexes with a free O–H group at the periphery of the antenna available for the potential phosphorylation reaction with OP nerve agents (P–X bond). The strategy is motivated from the irreversible nucleophilic attack of the serine hydroxyl group on the OP nerve agents at the active site of AChE (Scheme 1). The use of reactive hydroxyl groups in the molecular design of inorganic and organic optical probes for intended changes in the optical parameters for the detection of nerve agents/simulants has been documented.[19,24,25] The thermodynamically stable luminescent Eu(III)-complexes **Eu(*o*-OH)** and **Eu(*p*-OH)** exhibit highly intense red emission in solution and the solid state. The *o*- and *p*-hydroxyphenyl derivatives of imidazophenanthroline ligands (***o*-HPIP**, ***p*-HPIP**) containing reactive –OH groups were intentionally positioned to interact with DCP as the nerve agent mimic. The anionic β-diketonate ligand (TTA) is used to impart thermodynamic stability and charge neutralization *via* stronger ionic interactions with the hard Eu(III) centre. Both Eu(III)-probes show a selective 'turn-off' luminescence response towards DCP in the presence of various other competitive interferents. The 'turn-off' probes were responsive up to the ppb level for DCP [LOD: **Eu(*o*-OH)**, 18 ppb, **Eu(*p*-OH)**, 10 ppb]. We can also detect DCP in the nanomolar range in solution by the naked eye. The reactions of the Eu(III)-probes with DCP were monitored using ^{1}H-NMR titration studies using the diamagnetic isostructural control compound [La(***o*-HPIP**)$(TTA)_3$] [**La(*o*-OH)**] to define a probable luminescence quenching pathway. The final thermodynamically driven reaction product was structurally identified and showed possible hydrolysis reaction and degradation of the probe. For practical use, vapor phase detection of the OP simulants was carried out using the Eu(III)-probes immobilized on a low-cost filter paper strip showing distinct response and selectivity towards DCP.

Results and discussion

Synthesis and general aspects

The hydroxy-phenyl substituted-2-imidazophenanthroline ligands (***o*-HPIP**, ***p*-HPIP**) were synthesized using the well-known Debus–Radziszewski imidazole formation reaction *via* direct condensation of 1,10-phenanthroline-5,6-dione with *ortho*- and *para*-hydroxybenzaldehydes in glacial AcOH with an excess of NH_4OAc.[36] The rationale behind the *o*/*p*-isomer was to get insight into the effect of potential intramolecular hydrogen bonding in modulating the triplet-state of the ligands in sensitizing Eu(III) luminescence and the difference in reactivity for the nucleophilic attack to form phosphorylated ligands. The **Eu(*o*-OH)** and **Eu(*p*-OH)** complexes were synthesized using a stoichiometric ratio of 1 : 1 : 3 of Eu(III) : ***o*/*p*-HPIP** : TTA^- in MeOH under reflux for 12 h *via* metal-based template synthesis (Scheme 2).

Analogous diamagnetic [**La(*o*-OH)**] was prepared using a similar modular approach, anticipating identical types of bonding and coordination geometry around Ln(III). The three anionic β-diketonate ligands (2-thenoyltrifluoroacetonate (TTA)) were suitable to form stronger ionic bonds with the hard Ln(III), thereby satisfying coordinative saturation with enhanced thermodynamic stability and minimizing undesirable fast solvent-exchange reactions in solution. The

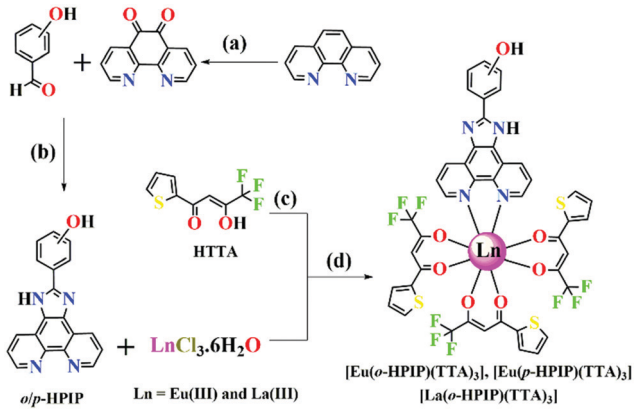

Scheme 2 Generalized synthetic scheme of the probes: **[Eu(*o*-OH)]**, **[Eu(*p*-OH)]**, and **[La(*o*-OH)]**. (a) H_2SO_4, HNO_3, KBr, 24 h at RT. (b) CH_3COOH, NH_4OOCH_3, reflux for 4 h. (c) NaOH in methanol. (d) Methanol, reflux for 12 h.

coordinative saturation (C.N. = 8) ensures their structural integrity in solution and minimizes luminescence quenching *via* vibrational energy transfer (VET) mediated by fast exchange reactions. The **Eu(*o*-OH)** and **La(*o*-OH)** complexes were structurally characterized using single-crystal X-ray diffraction, demonstrating their anticipated isostructural $\{LnN_2O_6\}$ square-antiprismatic coordination geometry. The complexes were characterized by FT-IR, ESI-MS, electronic absorption, and emission spectroscopy, supporting the formation of discrete molecular species in the solid state and solution. The ESI-MS spectral analysis of **Eu(*o*-OH)** reveals $[M-H^+]^-$ molecular ion peaks with the corresponding matching isotopic distribution patterns of the Eu(III) cations (Fig. S1 in the ESI†). In the FT-IR spectra of the complexes, $\nu_{C=O}$ stretching vibrations were present at ~1600 cm^{-1} compared to the free TTA at ~1650 cm^{-1}. The $\nu_{C=N}$ vibration bands in the complexes were observed at ~1539 cm^{-1} and ν_{C-F} bands at ~1140 cm^{-1}. The ν_{Eu-O} stretching bands in the complexes were observed at ~580 cm^{-1}, which suggests the coordination of the ligands with Eu(III) ions (Fig. S2 and S3 in the ESI†). Electronic absorption spectroscopy shows the absorption bands characteristic of the HPIP and TTA ligands in the complexes at 275, 296 nm, and 335 nm unperturbed by the Ln(III) ion (Fig. 3a). The emission spectroscopy shows the characteristic f → f transitions of Eu(III) with bright red luminescence originating from $^5D_0 \rightarrow {}^7F_J$ transitions (J = 0–4) (Fig. 3b). To evaluate the reactivity of the Eu(III) probes with DCP using NMR spectroscopy, isostructural diamagnetic **[La(*o*-OH)]** was used to avoid the broad spectrum and paramagnetic shifts in ^1H signals induced by paramagnetic Eu(III) complexes.[37] Thermogravimetric analysis shows that the probes withstand heat up to 250 °C, not losing any significant weight, indicating their stability in the solid state (Fig. S4 in the ESI†).

Structural characterization

The discrete isostructural mononuclear **Eu(*o*-OH)** and **La(*o*-OH)** complexes crystallized in the triclinic $P\bar{1}$ space group. Eu(III) and La(III) ions are coordinated to one N,N′-donor imidazophenanthroline (***o*-HPIP**) and three mono-anionic ancillary O,O′-donor 2-thenoyltrifluoroacetonate (TTA^-) ligands neutralizing the +3 charge of Ln(III) *via* ionic bonding. The disposition of ***o*-HPIP** and TTA^- results in eight-coordinated $\{LnN_2O_6\}$ polyhedra around the Ln(III) ions with distorted square-antiprismatic (SAP) geometry (Fig. 2b). The twist angle between the two square-planes is 40° for **Eu(*o*-OH)** and 41° for **La(*o*-OH)** compared to the ideal value of 45°. The peripheral phenyl-hydroxyl group at the *ortho*-position of the ***o*-HPIP** ligand is involved in a strong intramolecular [H–O···N, 1.88 Å in **Eu(*o*-OH)** and 1.87 Å in **La(*o*-OH)**] hydrogen bonding interaction with the free nitrogen on the imidazole by forming a six-membered ring. The exposed phenyl-hydroxy group is readily accessible as a reactive site for nucleophilic attack at positively polarized organophosphates. The Ln–O bond distances are 2.34–241 Å in **Eu(*o*-OH)** and 2.44–2.53 Å in **La(*o*-OH)**, tracking the trend in ionic sizes of Eu(III) and La(III). The shorter Ln–O bonds from TTA^- possess more ionic character than the Ln–N bonds from the neutral ***o*-HPIP** ligand. The ORTEP views of the complexes are shown in Fig. 2a and c. The unit cell packing diagrams, refinement parameters, selected bond lengths, and bond angles are shown in Fig. S5, S6 and Tables S1, S2 in the ESI,† respectively.

Photophysical characterization

The electronic absorption and emission spectra of the probes **Eu(*o*-OH)** and **Eu(*p*-OH)** were recorded in acetonitrile solution

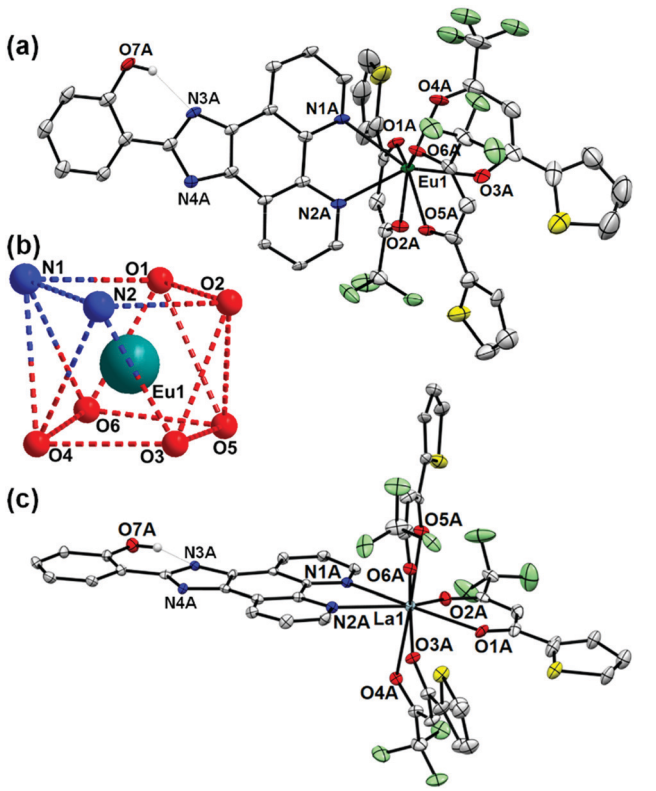

Fig. 2 The ORTEP view of **Eu(*o*-OH)** (a) and the $\{EuN_2O_6\}$ coordination polyhedra showing a square-antiprismatic (SAP) geometry (b). The ORTEP view of the isostructural diamagnetic **La(*o*-OH)** complex (c). Dotted lines show the intramolecular H-bonding in the HPIP ligand.

(5 μM) at 298 K. The complexes show three strong absorption bands at 275 nm [ε/M^{-1} cm^{-1}] = 51 800 [**Eu(*o*-OH)**], 53 800 [**Eu(*p*-OH)**]; 296 nm [ε/M^{-1} cm^{-1}] = 42 600 [**Eu(*o*-OH)**], 50 900 [**Eu(*p*-OH)**] and 336 nm [ε/M^{-1} cm^{-1}] = 63 600 [**Eu(*o*-OH)**], 53 600 [**Eu(*p*-OH)**] resulting from the ligand-centered transitions desirable for effective light-harvesting and sensitization of Eu(III) (Fig. 3a). The N,N-donor ligands show absorption bands in the 270–400 nm range with a major band centered at ~280 nm attributed to the intra-ligand (IL) π–π* transitions from the imidazophenanthroline derivatives.[38] The O,O-donor β-diketonate ligand TTA has an absorption maximum at ~330 nm assigned to π–π* transitions of the enol form.[39] The absorption bands of the complexes could be assigned to ligand-centered absorptions with an extensive overlap and minor shifts in band maxima. The absorption spectra of the coordinated ligands were minimally perturbed upon coordination to the Eu(III) ion, which has valence shell electrons in deeply buried f-orbitals, suggesting predominantly ionic bonding. An overlay of the absorption spectra of all the ligands (***o*/*p*-HPIP** and TTA), $Eu(TTA)_3{\cdot}2H_2O$, and the complexes is shown in Fig. S8 in the ESI.†

The PL spectra of **Eu(*o*-OH)** and **Eu(*p*-OH)** (5 μM) were recorded at the lowest energy absorption bands (λ_{ex} = 340 nm) showing emission resulting from the $^5D_0 \rightarrow {}^7F_0$ (580 nm), $^5D_0 \rightarrow {}^7F_1$ (592 nm), $^5D_0 \rightarrow {}^7F_2$ (613 nm), $^5D_0 \rightarrow {}^7F_3$ (653 nm), and $^5D_0 \rightarrow {}^7F_4$ (704 nm) transitions characteristics of Eu(III) ions. The induced electric-dipole allowed hypersensitive $^5D_0 \rightarrow {}^7F_2$ transitions at 613 nm, which is the most intense band compared with the others and primarily responsible for the bright red luminescence of both complexes. Moreover, it also suggests that a highly polarizable environment exists in the complexes around the Eu(III) ion.[40] The intensity ratio of I_{7F2}/I_{7F1} [18 for **Eu(*o*-OH)** and 17 for **Eu(*p*-OH)**] suggests a lack of inversion center of symmetry (C_i) around the Eu(III) ion (Fig. 3b).[41] The steady-state emission spectrum of **Eu(*o*-OH)** shows complete quenching of the ligand-centered emission and a very weak broad emission band at ~450 nm appears for **Eu(*p*-OH)** assigned to the ***p*-HPIP** ligand after excitation at the ligand-centered absorption band. This indicates that the photosensitized ligands effectively transfer energy (EnT) to the Eu(III) ion to populate the emissive excited $^5D_0$ state, followed by subsequent relaxation to the ground ^7F_J (J = 0–4) states resulting in bright luminescence (Fig. 3b).[42] The excitation spectra of the complexes recorded at 613 nm ($^5D_0 \rightarrow {}^7F_2$) overlap with the absorption spectra of both ligands, and they do not contain any Eu(III)-centered intrinsic sharp absorption peaks, suggesting very ineffective direct excitation as shown in Fig. S9 in the ESI.† This further supports the efficient indirect EnT from the dual antenna that populates the excited $^5D_0$ states of the Eu(III) ion. The reversible equilibria and binding of the neutral HPIP diimine ligand in $[Eu(HPIP)(TTA)_3]$ complexes containing ***o*/*p*-HPIP** and TTA ligands in a 1 : 3 ratio were established by quantitative luminescence titration studies.[43,44] We took $Eu(TTA)_3{\cdot}2H_2O$ as a precursor for $[Eu(HPIP)(TTA)_3]$ complexes, titrated with ***o*/*p*-HPIP**, and recorded the photoluminescence spectra as shown in Fig. 4a and b. The inset plot shows the enhancement in the Eu(III) emission intensity with increasing [***o*/*p*-HPIP**] until reaching a 1 : 1 molar ratio with $Eu(TTA)_3{\cdot}2H_2O$, confirming the formation of the coordinatively saturated $[Eu(HPIP)(TTA)_3]$ formulation. After reaching this saturation level, further addition of [***o*/*p*-HPIP**] does not cause any apparent changes in luminescence intensity. These observations suggest that Eu(III) is coordinated to one N,N′-donor and three TTA ligands and exists as eight-coordinated [Eu(***o*/*p*-HPIP**)$(TTA)_3$] in solution. The binding constants (K_b) of the ligands [7.82 × 10^5 M^{-1} for ***o*-HPIP** and 6.59 × 10^5 M^{-1} for ***p*-HPIP**] were calculated from the above luminescence titration studies, which suggest the significant stability of the **Eu(*o*-OH)** and **Eu(*p*-OH)** complexes in solution. The luminescence decay lifetimes (τ) of the complexes for the $^5D_0 \rightarrow {}^7F_2$ transition (613 nm) were calculated from their decay curves in acetonitrile. The τ values for **Eu(*o*-OH)** and **Eu(*p*-OH)** were 570 μs and 520 μs, respectively, compared to the labile $Eu(TTA)_3{\cdot}2H_2O$ (τ ~ 280 μs). These decay curves fit well with the mono-exponential equation and confirm the presence of [Eu(***o*-/*p*-HPIP**)$(TTA)_3$] as the predominant species existing in solution (Fig. 4c). Further speciation studies

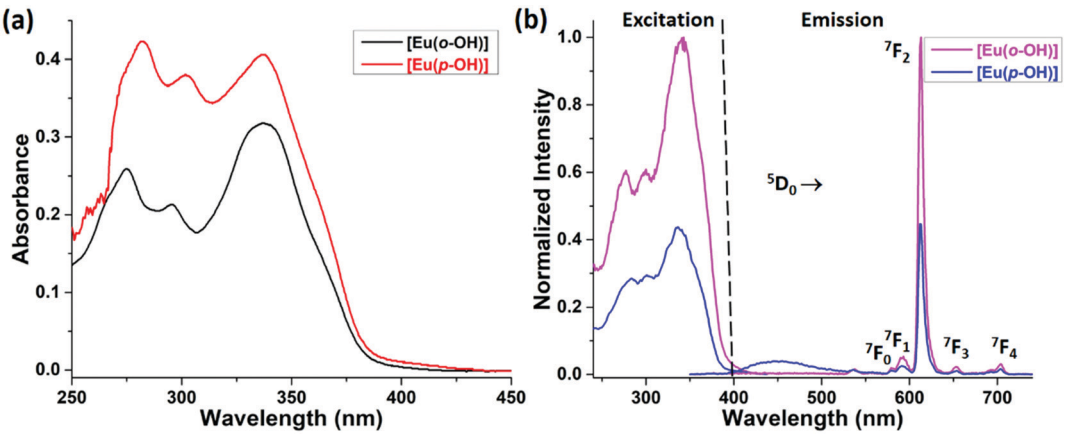

Fig. 3 (a) Electronic absorption spectra of the complexes **Eu(*o*-OH)** and **Eu(*p*-OH)** (5 μM) in MeCN at 298 K. (b) Excitation spectra of the complexes **Eu(*o*-OH)** and **Eu(*p*-OH)** (5 μM) recorded at λ_{em} = 613 nm and their PL spectra showing the characteristic $^5D_0 \rightarrow {}^7F_J$ transitions for Eu(III) at λ_{ex} = 340 nm. Ex./Em. slit width = 5 nm.

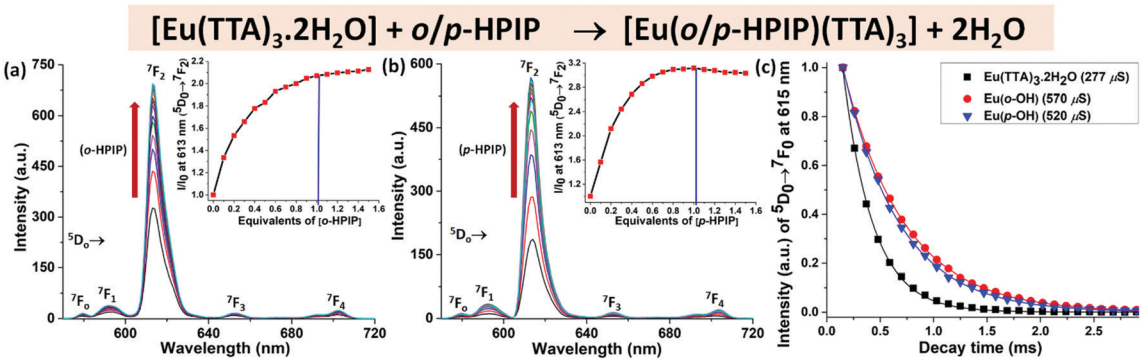

Fig. 4 (a) Enhancement of the luminescence intensity of $Eu(TTA)_3{\cdot}2H_2O$ (5 μM) with increasing concentration of ***o*-HPIP**. Inset: Changes in relative emission intensity for the $^5D_0 \rightarrow {}^7F_2$ transition with equiv. of ***o*-HPIP** added. (b) Enhancement of the luminescence intensity of $Eu(TTA)_3{\cdot}2H_2O$ (5 μM) with increasing concentration of ***p*-HPIP**. Inset: Changes in relative emission intensity for the $^5D_0 \rightarrow {}^7F_2$ transition with equiv. of ***p*-HPIP** added. (c) Luminescence decay profile of the $^5D_0 \rightarrow {}^7F_2$ transition used for lifetime measurements for the complexes **$Eu(TTA)_3{\cdot}2H_2O$**, **Eu(*o*-OH)** and **Eu(*p*-OH)** in MeCN (5 μM) at 298 K. λ_{ex} = 340 nm, delay time and gate time = 0.1 ms, total decay time = 10.0 ms, Ex. and Em. slit width = 5 nm.

were carried out on the probes, and their hydration numbers (q) were calculated from the luminescence decay time in H_2O (τ_{H2O}) and D_2O (τ_{D2O}) (Fig. S10 and S11 in the ESI†). The calculated q values were close to zero, which directly supports the absence of the inner-sphere coordinated water/solvent molecule to the Eu(III) ion and achievement of coordinative saturation (C.N. = 8).[45] After studying the solution speciation of the probes, we proceed to study the interactions of the analytes.

Detection of the DCP nerve agent mimic in solution

The electronic absorption and photoluminescence spectra of the probes (5 μM) were recorded with gradual addition of the analyte in solution. Before the experiments, solutions of the probes and analytes were prepared in degassed solvents. The ligand-centered (π–π*) absorption bands of the probe **Eu(*o*-OH)** at 296 and 336 nm display significant changes with increasing concentration of DCP. A decrease of these bands with the addition of DCP (0–15 μM) was observed with the concomitant appearance of two new bands at 314 and 328 nm with a clear isosbestic point at 322 nm (Fig. 5a). No further changes in the absorption spectra were noticed after the addition of 3 equiv. of the OPs. A similar response was observed in the absorption spectra of **Eu(*p*-OH)** with the addition of increasing amounts of DCP. Addition of DCP (0–10 μM) results in the decrease of intensity at

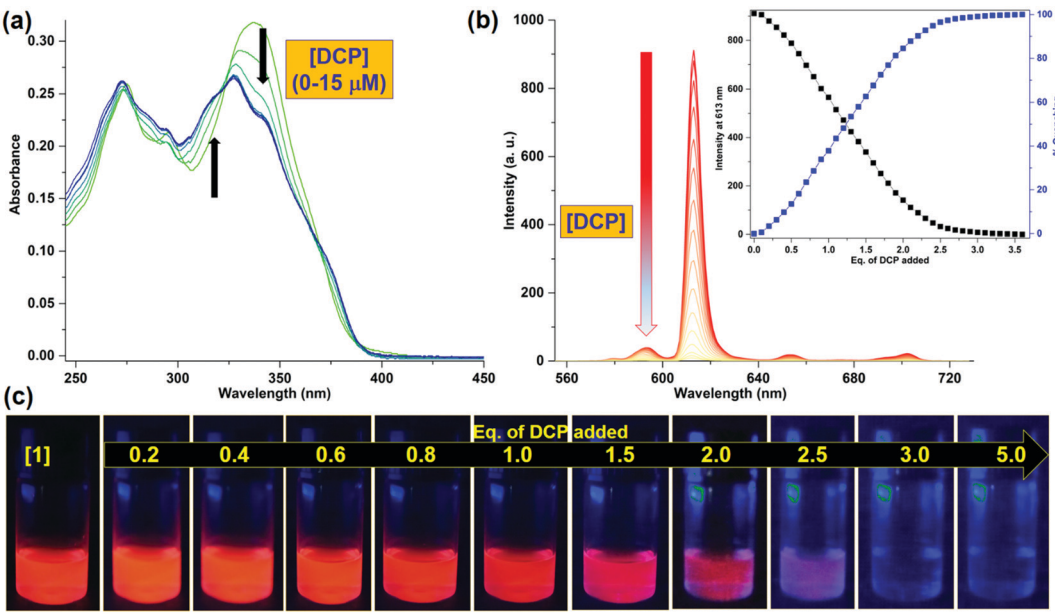

Fig. 5 (a) Changes in the electronic absorption spectra of **Eu(*o*-OH)** (5 μM) with increasing concentration of DCP (0–15 μM) in MeCN at RT. (b) Changes in the PL spectra (λ_{ex} = 340 nm) of **Eu(*o*-OH)** (5 μM) with the addition of increasing amounts of DCP (0–15 μM) observed for the characteristic emission from the hypersensitive band of the Eu(III) ion ($^5D_0 \rightarrow {}^7F_2$ = 613 nm). Inset: Plot showing the quenching of PL intensity and percentage quenching of emission at 613 nm *vs.* the equivalents of DCP added. (c) Digital images showing quenching of the bright red-luminescence of **Eu(*o*-OH)** (5 μM) with varying equivalents of DCP (0.2–5.0 equiv.) under 365 nm UV-A light.

296 and 336 nm and the appearance of a new band at 314 nm with an isosbestic point at 324 nm for **Eu(*p*-OH)** (Fig. 6a). The presence of one isosbestic point with concomitant appearance of new bands in both probes suggests the formation of new species with the addition of OPs in solution.

The selective response of DCP, which is a sarin (GB) simulant with a relatively lower toxicity,[46] was evaluated with the luminescent Eu(III) probes using the time-delayed photoluminescence intensity originating from the f → f transitions as a sensitive spectroscopic yardstick in solution. Quenching of the intense red emission of Eu(III) ($^5D_0 \rightarrow {}^7F_J$, J = 0–4) from the complexes was observed with the addition of DCP. As shown in Fig. 5b, significant irreversible quenching of the characteristic emission of the Eu(III) in the probe **Eu(*o*-OH)** (5 μM) results from the gradual addition of DCP (0–15 μM). The luminescence was nearly turned off upon the addition of ~3 equiv. of DCP, and no further changes were noticed upon excess addition of DCP. This is evident from the inset plot in Fig. 5b, which shows the relative quenching of the hypersensitive band ($^5D_0 \rightarrow {}^7F_2$) for Eu(III) at 613 nm with a molar equivalent of DCP added. Before drawing any conclusion from the above observations, we examined whether the emission quenching is solely triggered by DCP or due to possible hydrolyzed products, considering its susceptibility towards such hydrolysis. HCl might be present in the DCP solution as an impurity at a minute concentration due to its hydrolysis, which might cause such quenching of luminescence. To gain insights into this reaction, we recorded the luminescence of **Eu(*o*-OH)** (5 μM) in both acidic and basic media and observed slow quenching of emission upon going to either acidic or basic ranges from the neutral condition by titrating with HCl or Et_3N/NaOH (Fig. S12–S15 in the ESI†). Further, upon maintaining the neutral pH, the luminescence was almost completely regained (Fig. S14 in the ESI†). Such reversible changes in emission intensity indicate that the quenching caused by acid or base is reversible in nature due to possible displacement of pH-sensitive TTA or protonation and deprotonation of the donor-N of HPIP ligands. Complete luminescence quenching is achieved by adding 3.0 equivalents of DCP and is irreversible. From these observations, we presume that the quenching of the emission of the probes in our experiments is caused by interaction with DCP and moved on to detailed studies with these probes.

The bright red luminescence quenching of the probe (5 μM) in solution could be visualized under 365 nm UV-A light with increasing concentration of DCP (Fig. 5c). The PL spectrum of the probe **Eu(*p*-OH)** shows similar changes after titration with DCP. Quenching of the characteristic emission band was observed, and it continues until 'turn-off' luminescence appeared with the addition of ~2 equiv. of DCP (Fig. 6b and c). The differential luminescence quenching rates for the probes **Eu(*o*-OH)** (~3 equiv. of DCP) and **Eu(*p*-OH)** (~2 equiv. of DCP) in the presence of DCP under identical conditions suggest that the analyte differentially reacts with the probes in solution. The reaction rate is affected by the specific molecular design of the probe (*i.e.* position of the –OH group in phenyl ring). Both the Eu(III) probes were found to be selective towards the DCP nerve gas simulant when tested in the presence of other OP interferents (*e.g.*, DECP, DMMP, DEPP). Except for DECP, which causes little luminescence quenching only at high concentrations, other interfering OPs do not cause any

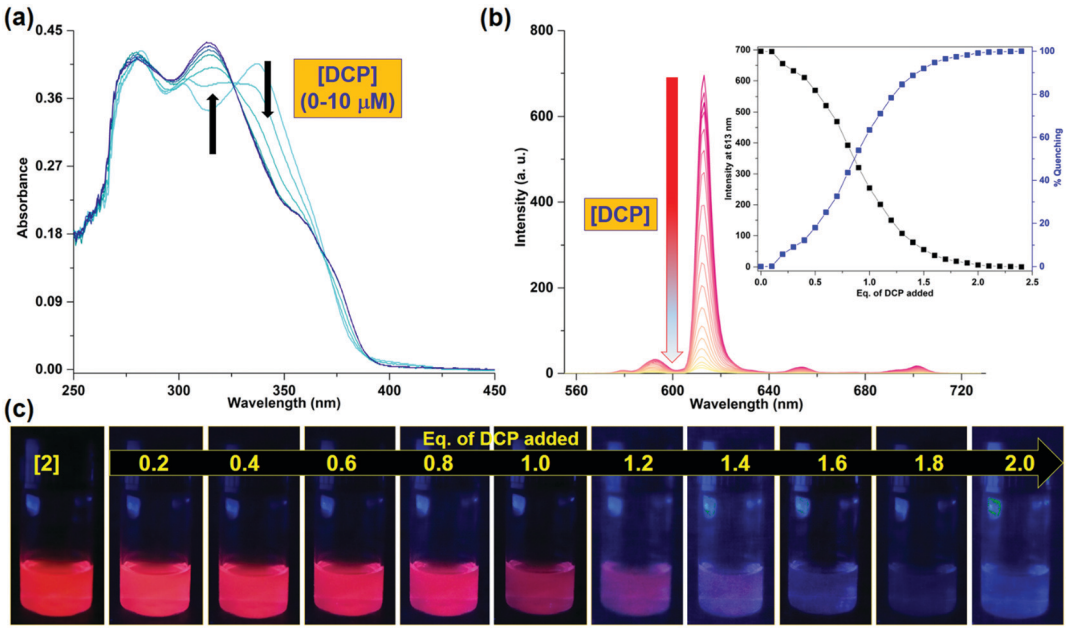

Fig. 6 (a) The changes in the electronic absorption spectra of **Eu(*p*-OH)** (5 μM) with increasing concentration of DCP (0–10 μM) in MeCN. (b) The changes in the PL spectra (λ_{ex} = 340 nm) of **Eu(*p*-OH)** (5 μM) with the addition of increasing amounts of DCP (0–10 μM) observed for the characteristic emission from the hypersensitive band of the Eu(III) ion ($^5D_0 \rightarrow {}^7F_2$ = 613 nm). Inset: Plot showing the quenching of PL intensity along with percentage quenching of emission at 613 nm *vs.* the equivalents of DCP added. (c) Digital images showing quenching of the bright red luminescence of the probe **Eu(*p*-OH)** (5 μM) with varying equivalents of DCP (0.2–2.0 equiv.) under 365 nm UV-A light.

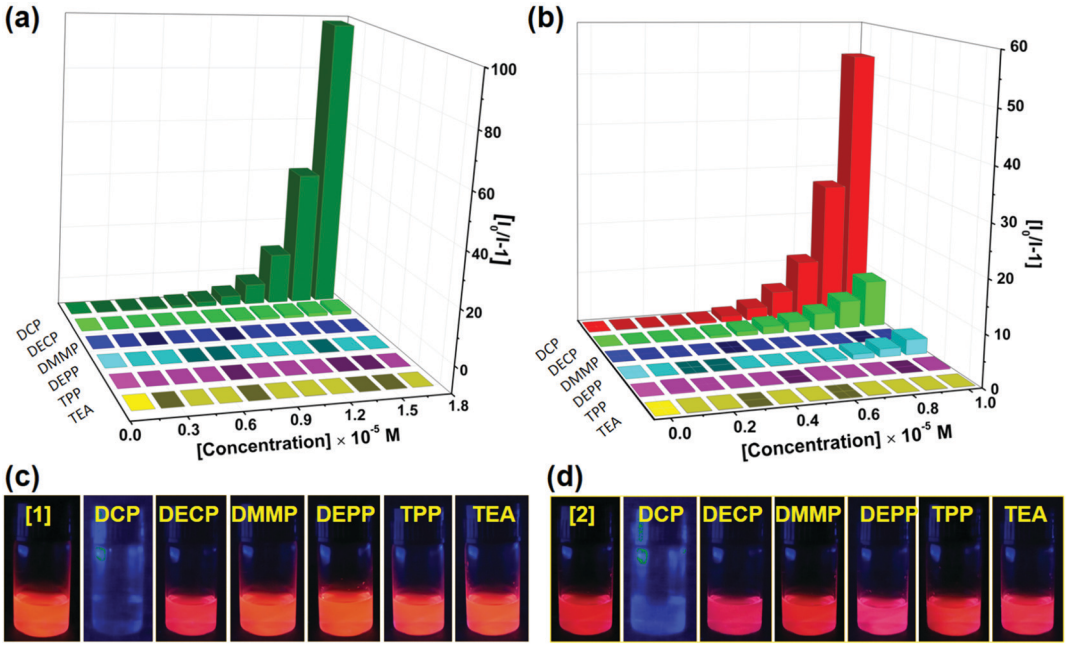

Fig. 7 The luminescence response (λ_{ex} = 340 nm) of the probes (a) **Eu(*o*-OH)** and (b) **Eu(*p*-OH)** (5 μM) in the presence of various OP reagents. OPs: DCP (diethyl chlorophosphonate), DECP (diethyl cyanophosphonate), DMMP (dimethyl methylphosphonate), DEPP (diethyl phenylethylphosphonate), TPP (triphenyl phosphonate), and TEA (triethylamine). The digital images showing responses in the red luminescence of (c) **Eu(*o*-OH)** and (d) **Eu(*p*-OH)** (5 μM) with DCP and other interferents (DECP, DMMP, DEPP, TPP, and TEA in MeCN visualized under 365 nm UV-A light.

quenching of the luminescence of the Eu(III) probes in similar experimental conditions (Fig. 7a and b). The digital images of the probe solutions with nerve agent simulants and various OP interferents under UV-A light (λ = 365 nm) show the selective 'turn-off' luminescence response for DCP (Fig. 7c and d). We observed a comparatively higher selectivity of the **Eu(*o*-OH)** probe for DCP, which involves a strong intramolecular hydrogen bonding between the hydroxyl group and a nitrogen atom of the imidazole ring (Fig. 2). The high reactivity of the P–Cl bond with the nucleophilic *o*-OH group presumably results in quenching of the luminescence of **Eu(*o*-OH)** selectively. The **Eu(*p*-OH)** probe is not involved in such intramolecular H-bonding and has a readily available *p*-OH group to interact with OPs having reactive P–X (X = Cl and CN) bonds. **Eu(*o*-OH)** is highly selective to DCP with a more reactive P–Cl bond than the less reactive P–CN bond of DECP, showing anticipated reactivity differences of the OPs with the free OH group of the ***p*-HPIP** ligand in similar conditions. The **Eu(*p*-OH)** probe was found to be more sensitive due to the presence of free *p*-OH and showed complete luminescence quenching even with 2 equiv. of DCP, while **Eu(*o*-OH)** with an *o*-OH group involved in intramolecular H-bonding shows complete quenching with 3 equiv. of DCP. These results suggest that selective and sensitive detection of DCP is effectively possible with the tested luminescent Eu(III) probes in solution by varying the reactivity of the functional groups. The **Eu(*o*-OH)** probe was found to be highly selective for DCP, while the **Eu(*p*-OH)** probe is selective as well more sensitive toward DCP.

A few luminescent Ln(III) probes for nerve agents or their simulants showing quenching (turn-off) were reported. Such 'turn-off' triggering was observed due to competitive displacement of the sensitizing antenna or phosphorylation of the sensitizing ligand at the Ln(III)-coordination site and subsequent decomplexation.[35,47,48] We have reported a terpyridine-dicarboxylate based Eu(III) probe as a turn-on sensor for DCP based on minimizing non-radiative vibrational energy-transfer, which demonstrated significant enhancement of the $^5D_0 \rightarrow {}^7F_2$ transition.[32] The calculated limit of detection (LOD) was 18 ppb (110 nM) for **Eu(*o*-OH)** and 10 ppb (56 nM) for **Eu(*p*-OH)**. The selective detection of G-series nerve agent simulants in the ppb range is immensely encouraging using highly sensitive TRL as a spectroscopic tool that is devoid of autofluorescence and photobleaching, which is superior to organic fluorophores. Only a few optical probes for nerve agents (or simulants) have been reported in the literature for their detection at the ppb level.[35]

Herein we attempted to explore the possible mechanism or underlying reactions between the DCP and reactive-OH containing emissive Ln(III) probes using ^{1}H-NMR spectroscopy. We studied the reactivity of DCP with the diamagnetic analog **La(*o*-OH)** in DMSO-d_6 instead of the paramagnetic **Eu(*o*-OH)** using ^{1}H-NMR titration to avoid broadening of the ^{1}H-NMR peaks.[37] We noticed two new peaks in the aliphatic region at 1.20 ($-CH_3$) as a triplet and 3.80 ppm ($-CH_2$) as a quartet belonging to the ethyl group of DCP along with upfield and downfield shifts of the ^{1}H signals in the aromatic region corresponding to both ***o*-HPIP** and TTA antenna chromophores (Fig. S16–S18 in the ESI†). After addition of one equiv. of DCP, the peaks at 13.97 ppm (–OH) and 12.60 ppm (–NH) disappeared, suggesting the possible interaction (*i.e.*, phosphorylation reaction) of these groups with the organophosphates (Fig. S18 in the ESI†).

Addition of one equivalent of DCP causes only partial quenching of luminescence and further addition leads to complete 'turn-off' luminescence. The NMR titration data were not sufficient to explicitly propose the intricate luminescence quenching mechanism involving multiple energy transfer steps to sensitize the Eu(III) ion. Only a very limited reports exist on the ultimate products formed over time upon reactions of the Ln(III) sensors and such nerve agent mimics. To unambiguously confirm the identity of the final thermodynamically stable product(s), we attempted to crystallize the reaction product of the probe **Eu(*o*-OH)** and DCP (5 equiv.) by mixing them in $CHCl_3$. The structure obtained after a prolonged time by slow evaporation yields a linear polymeric chain containing Eu(III) ions and diethyl hydrogen phosphate (DHP) ($[\mathbf{Eu(DHP)_3}]_n$), a hydrolysis product of DCP, as shown in Fig. 8. A single polymeric chain unit contains two Eu(III) ions bridged by three diethyl phosphate anions (Fig. S7 in the ESI†). Each Eu(III) ion is coordinated to six O-atoms of the six DHP molecules. Based on the literature and our observations from differential emission quenching rates of the probes, NMR titration with DCP and identification of the hydrolyzed Eu-DHP polymeric product, we could only propose a possible luminescence quenching mechanism. The exact sequence of chemical reactions and their speciation in solution is difficult to establish considering the fast substitution kinetics, reactivity and adventitious hydrolysis of DCP and the ionic bonding nature of the Eu(III) probes. The proposed mechanistic pathway involves a possible phosphorylation reaction at the ligand periphery *via* nucleophilic attack by the OH group of the ***o*/*p*-HPIP** ligand at the reactive P–Cl bond of DCP, followed by hydrolysis of the intermediate phosphorylated moiety, which leaves diethyl hydrogen phosphate (DHP) as a product.[50–53] However, we could not completely ignore the *in situ* hydrolysis of the reactive DCP in the presence of traces of water or moisture to form DHP. DHP is a strong oxoacid and ideal for coordination with the hard Lewis acid Eu(III) by removing the sensitizing antenna from the coordination sphere (Scheme 3). This reaction yields a thermodynamically stable product, $[\mathbf{Eu(DHP)_3}]_n$, as a linear polymeric chain as shown in Fig. 8 and Fig. S7 (ESI†). The absence of any antenna effect for sensitizing Eu(III) due to changes in the coordination sphere (*i.e.*, displacement/chemical alteration of antenna ligands) causes the quenching of the "luminescence of the probes with literature precedence (Scheme 3).[35,47–49,53–56]

Vapor phase detection of DCP in a solid-state film

Fluorescence-based solution-phase detection of nerve agents using various optical sensors is well-studied compared to their vapor phase detection in the solid phase for designing practical detection kits. Vapor phase detection is highly desirable for practical applications considering their volatile nature. Apparently, inconspicuous volatile colorless and odorless nerve agents could be spread as aerosols. Because of their higher density than that of air, they remain near the ground, which makes them more lethal and their timely detection more challenging.[57] Therefore, the on-site detection of these nerve gases in the vapor phase using simple, selective and sensitive low-cost solid-state sensors is crucial to mitigate real threat scenarios for public health. Herein, to test this requirement, we used a low-cost filter paper strip as a solid-state matrix and impregnated it with the luminescent probes **Eu(*o*-OH)** and **Eu(*p*-OH)**. The sensor-loaded air-dried filter paper strips show bright red luminescence due to the $^5D_0 \rightarrow {}^7F_2$ f–f transitions from Eu(III) ion under 365 nm UV-A irradiation (Fig. 9a). These Eu(III)-probe loaded filter paper strips were exposed to the vapors of the organophosphorus nerve agents and various interfering OPs and TEA (100 μL). Upon exposure to the DCP vapor inside long scintillation vials inside a well-ventilated fume-hood, the initial bright red luminescence of the filter paper strips was significantly quenched for both the tested probes (Fig. 9 and 10). Other interfering OPs do not show considerable quenching of the luminescence of the filter paper strip. This observation confirms that the Eu(III)-probes can selectively detect the presence of DCP vapors in the atmosphere using a simple, low-cost, filter-paper based solid-state sensor (Fig. 9a and 10a). The luminescence of the immobilized filter paper strip was also recorded by varying the concentration of DCP. Noticeable quenching of the bright red luminescence was observed even at lower concentrations of DCP (20 μL) and a total quenching or turn-off luminescence was observed with ~80 to 100 μL of DCP under similar conditions as shown in Fig. 9b and 10b. These observations apparently exhibit the dependency of the photoluminescence of the probe upon DCP vapor concentration in the solid-state matrix due to anticipated phosphorylation reactions with the hydroxyl-containing PIP-antenna as proposed in the solution phase.

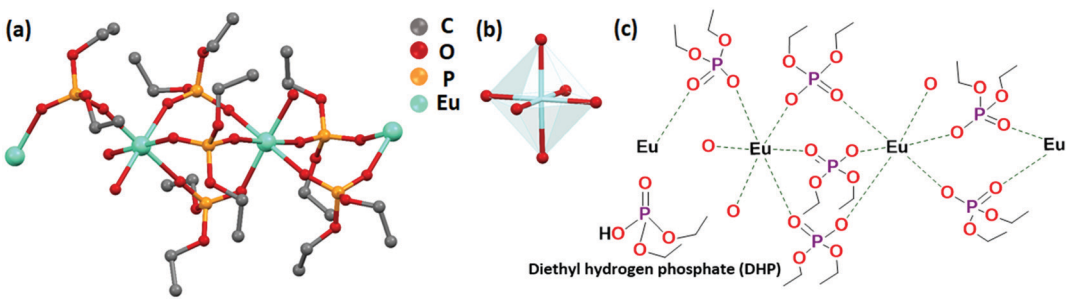

Fig. 8 (a) The molecular structure of a single unit from the 1D chain polymeric product $[\mathbf{Eu(DHP)_3}]_n$ obtained after a prolong reaction time of **Eu(*o*-OH)** with DCP. (b) Octahedral geometry acquired by the Eu(III) ion from coordinating O-atoms of DHP. (c) Schematic chemical drawing of a single unit of the polymeric product. Diethyl hydrogen phosphate (DHP) is shown at the bottom for clarity.

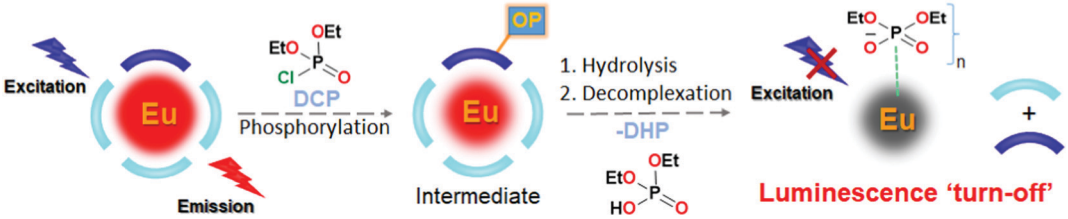

Scheme 3 A schematic diagram of the proposed reaction pathway for the interaction of Eu(III) probes with DCP leading to turn-off luminescence. One of the identified hydrolyzed end-products ($[Eu(DHP)_3]_n$) is shown in Fig. 8.

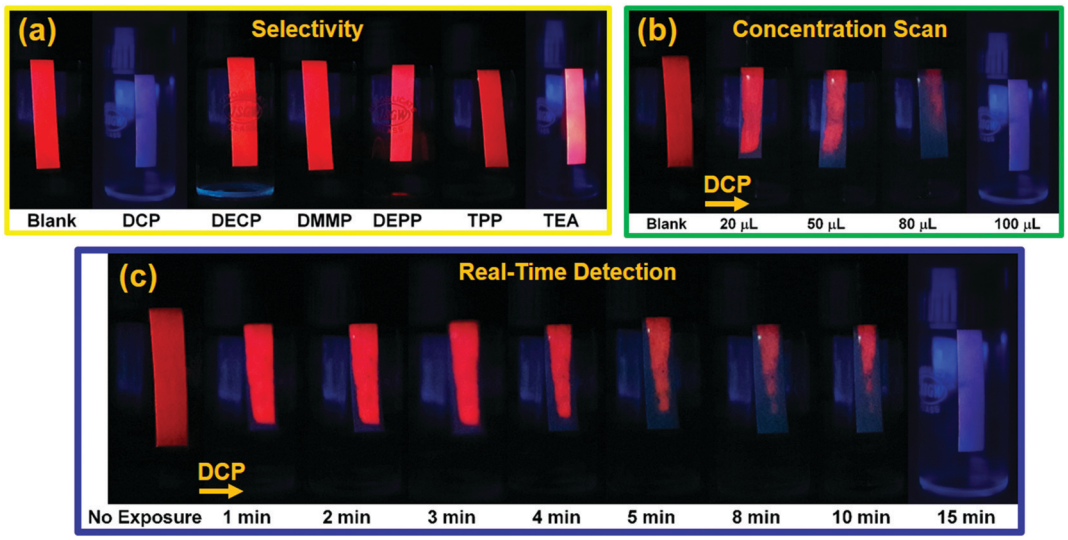

Fig. 9 (a) Selective response of the luminescence of **Eu(*o*-OH)** immobilized on filter paper strips in the presence of DCP vapors and vapors of other interferents (100 μL) under 365 nm UV-A exposure. (b) Quenching of the luminescence of **Eu(*o*-OH)** immobilized on paper strips upon exposure to increasing DCP concentration (0–100 μL). (c) The real-time response of the luminescence (time scan) of strips upon exposure to DCP vapors (100 μL).

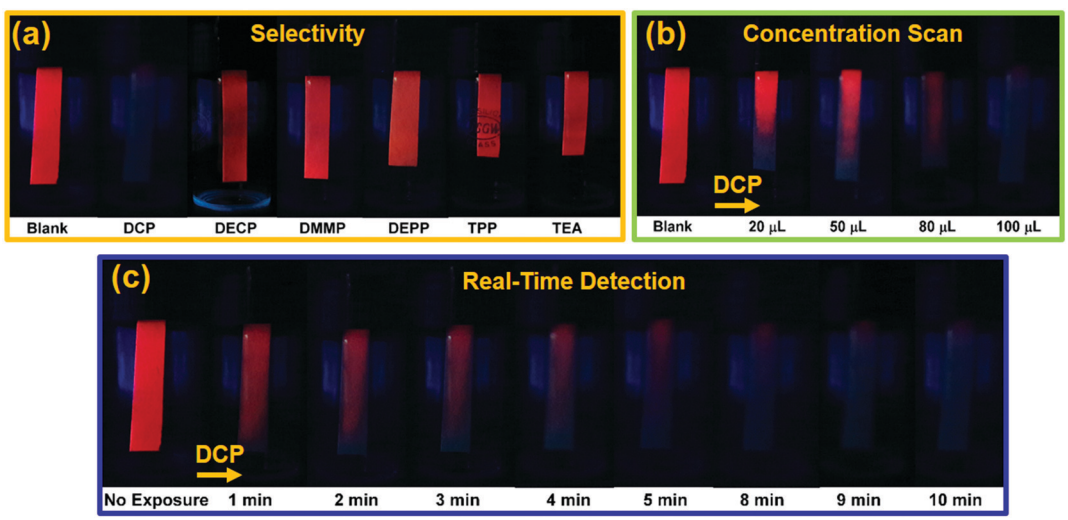

Fig. 10 (a) Selective response of the luminescence of **Eu(*p*-OH)** immobilized on filter paper strips in the presence of DCP vapors and vapors of other interferents (100 μL) under 365 nm UV-exposure. (b) Quenching of the luminescence of **Eu(*p*-OH)** immobilized on paper strips upon exposure to increasing DCP concentration (0–100 μL). (c) Real-time response of the luminescence of strips upon exposure to DCP vapors (100 μL).

Both the **Eu(*o*-OH)** and **Eu(*p*-OH)** probes work similarly towards the selective detection and concentration-dependent response in the presence of DCP vapor.

Finally, we also investigated the response-time of the probe by measuring the real-time photoluminescence of the probe immobilized on filter paper strips. Upon exposure to DCP vapor under 365 nm UV irradiation, gradual quenching of the luminescence of the filter paper strips with time was observed in both probes. The **Eu(*o*-OH)** probe took *ca.* 15 min for complete quenching of the luminescence, while it took *ca.* 10 min for the **Eu(*p*-OH)** probe on exposure to DCP vapor (100 μL) (Fig. 9c and 10c). The **Eu(*p*-OH)** probe is more sensitive and reacts faster towards DCP vapor, presumably due to the freely available *p*-OH group for nucleophilic attack, leading to complete quenching, while in **Eu(*o*-OH)**, where the *o*-OH is involved in intramolecular hydrogen bonding with the imidazole-N of HPIP takes a slightly longer time. These studies reveal that the tested simple solid-state Eu(III) probes are useful towards rapid selective naked-eye visualization of DCP vapor due to complete quenching of their photoluminescence intensity.

Experimental section

Synthesis and characterization

The imidazo-phenanthroline ligands (***o*-HPIP**, ***p*-HPIP**) were prepared using a modified literature procedure from the condensation of 1,10-phenanthraquinone and *o*/*p*-hydroxybenzaldehydes.[36]

2-(2-Hydroxyphenyl)imidazo[4,5-*f*][1,10]phenanthroline (*o*-HPIP). A mixture of phenanthroline-5,6-dione (100 mg, 0.48 mmol) and ammonium acetate (1.1 g, 14.4 mmol) was dissolved in glacial acetic acid (3 mL). To this reaction mixture, a solution of 2-hydroxybenzaldehyde (58.6 mg, 0.48 mmol) in 2 mL acetic acid was added and refluxed for 4 h. The reaction was quenched with water (50 mL), and then aqueous ammonia solution was added for neutralization, which results in a yellow precipitate. The precipitate was collected after filtration, washed with a copious amount of water and then with a small volume of ethanol, and dried in vacuum to obtain the desired ligand in 45% yield. ^{1}H-NMR (500 MHz, DMSO-d_6), δ (ppm): 13.98 (s, 1H), 12.75 (s, 1H), 9.09 (dd, 2H, $J1$ = 4.4 Hz, $J2$ = 1.5 Hz), 8.98 (dd, 2H, $J1$ = 7.8 Hz, $J2$ = 1.5 Hz), 8.21–8.23 (m, 1H), 7.89 (dd, 2H, $J1$ = 7.8 Hz, $J2$ = 4.4 Hz), 7.41–7.45 (m, 1H), 7.11–7.14 (m, 2H). ESI-MS in MeOH: calcd m/z for $C_{19}H_{13}N_4O$ as $[M + H]^+$ = 313.109, found = 313.108.

2-(4-Hydroxyphenyl)imidazo[4,5-*f*][1,10]phenanthroline (*p*-HPIP). A procedure similar to that for ***o*-HPIP** was followed for the synthesis of this ligand. ^{1}H-NMR (500 MHz, DMSO-d_6), δ (ppm): 13.52 (s, 1H), 9.98 (s, 1H), 9.03 (dd, 2H, $J1$ = 4.4 Hz, $J2$ = 1.5 Hz), 8.91 (dd, 2H, $J1$ = 8.8 Hz, $J2$ = 1.5 Hz), 8.12 (d, 2H, J = 7.8 Hz), 7.83 (dd, 2H, $J1$ = 8.8 Hz, $J2$ = 4.4 Hz), 6.99 (d, 2H, J = 7.8 Hz). ESI-MS in MeOH: calcd m/z for $C_{19}H_{13}N_4O$ as $[M + H]^+$ = 313.109, found = 313.109.

[Eu(*o*-HPIP)(TTA)$_3$] [Eu(*o*-OH)]. One equivalent of $EuCl_3 \cdot 6H_2O$ (0.1 mmol, 52 mg) was stirred with ***o*-HPIP** (1 equiv., 0.1 mmol and 31.2 mg) for 1 h in 10 mL methanol. To this solution, a neutralized solution of TTA (3 equiv., 0.3 mmol and 66.6 mg) in methanol was added and refluxed for 12 h. The solvent was evaporated in vacuum and the solid product was redissolved in chloroform and filtered to remove salt impurities. The filtrate upon evaporation in vacuum yielded the desired complex **Eu(*o*-OH)**. The compound was crystallized in chloroform solution. Yield: 81% (92 mg). ESI-MS in $CHCl_3$ (m/z): $[M–H^+]^-$ calculated for $C_{43}H_{23}EuF_9N_4O_7S_3$ = 1126.980, found: 1126.983. UV-Vis in MeCN: (λ_{abs}/nm (ε/M^{-1} cm^{-1}): 273 (29 100), 340 (30 800). FT-IR (KBr/cm^{-1}): 3424 (br), 1674 (s), 1601 ($\nu_{C=O}$, s), 1539 (s), 1513 (s), 1485, 1465, 1412, 1357, 1307, 1248, 1230, 1190, 1141, 1080, 1035, 1032, 934, 859, 788, 768, 751, 720, 681, 669, 641, 581.

[Eu(*p*-HPIP)(TTA)$_3$] [Eu(*p*-OH)]. The synthesis of **Eu(*p*-OH)** was performed following a similar procedure to that used for complex **Eu(*o*-OH)**, but the ***p*-HPIP** ligand was used in place of ***o*-HPIP**. Yield: 75% (85 mg). ESI-MS in $CHCl_3$ (m/z): $[M + Na^+]^+$ calculated for $C_{43}H_{23}EuF_9N_4O_7S_3$ = 1126.980, found: 1126.983. UV-Vis in MeCN: (λ_{abs}/nm (ε/M^{-1} cm^{-1}): 273 (23 800), 340 (29 300). FT-IR (KBr/cm^{-1}): 3476 (br), 1675(m), 1602 ($\nu_{C=O}$, s), 1539(s), 1507, 1485, 1454, 1411, 1357, 1306, 1258, 1191, 1079, 1062, 1037, 934, 859, 842 789, 768, 721, 682, 642, 582, 518.

[La(*o*-HPIP)(TTA)$_3$] [La(*o*-OH)]. A procedure similar to that mentioned above was applied for the synthesis of this complex also using $LaCl_3 \cdot 6H_2O$ in place of the Eu(III) salt. Yield: 75% (85 mg). FT-IR (KBr/cm^{-1}): 1597 ($\nu_{C=O}$, s), 1534(s), 1502, 1480, 1450, 1410, 1353, 1296, 1245, 1183, 1129, 1059, 1035, 931, 858, 840, 785, 749, 716, 679, 639, 577. The compound was recrystallized from chloroform solution and structurally characterized by X-ray crystallography.

General and spectroscopic measurements

Fourier transform-infrared (FT-IR) spectra were recorded on a PerkinElmer model 1320 spectrometer with KBr disc in the 4000–400 cm^{-1} range and the NMR characterization and titration data were recorded on a JEOL 400/500 MHz spectrometer in deuterated solvents with reference to TMS at 298 K. The ESI-MS spectra of the compounds used here were recorded on a Q-TOF electrospray ionization mass spectrometer. Thermogravimetric analysis data were obtained from a Mettler Toledo Star System under a N_2 atmosphere with a heating rate of 10 °C min^{-1}. The absorption spectra of all ligands (5 μM) and complexes (5 μM) were recorded in MeCN on a Varian V670 spectrophotometer at 298 K. Responses to the addition of aliquots of the OP agents on the absorption bands of the complexes (5 μM) were monitored in acetonitrile. The luminescence of both complexes was recorded on an Agilent Cary Eclipse fluorescence spectrophotometer. Fluorescence assay measurements of complexes **Eu(*o*-OH)** and **Eu(*p*-OH)** (5 μM) were performed with the addition of aliquots of solutions of diethylchlorophosphate (DCP) or other OP interferants at an excitation wavelength (λ_{ex}) of 340 nm.

X-ray crystallography

The single-crystal X-ray diffraction data of the **Eu(*o*-OH)** and **La(*o*-OH)** complexes and the **Eu(DHP)** polymeric product were

collected on a Bruker D8 Quest Microfocus X-ray CCD diffractometer (ω scans) with Mo Kα radiation (λ = 0.71073 Å) at 100(2) K. Data frame collections, indexing of reflections, and lattice parameter determination were done using the SMART program, while the integration of the intensity of reflections and scaling were performed using the SAINT program.[58] Absorption corrections were done using SADABS[59] and the space group determination using SHELXTL programs.[60] Structure solution and refinement were done using the full matrix least square method against F^2 with SHELXT and SHELXL-2018/3 using the WinGX and Olex2 software systems.[61–63] The non-hydrogen atoms were refined until convergence was reached using anisotropic thermal parameters and riding model refinement was applied on all the hydrogen atoms to include them in their idealized positions. The perspective images of complexes **Eu(*o*-OH)** and **La(*o*-OH)** are shown in Fig. 2(a and b), respectively. The unit cell packing diagrams, crystallographic parameters, and significant bond lengths and angles of the complexes and **[Eu(DHP)$_3$]$_n$** are shown in Fig. S5–S7 and Tables S1–S3 in the ESI.†

Vapor phase measurements of DCP in a solid-state film

The paper-based strips were prepared by dipping evenly cut-out small-sized adsorbent Whatman filter paper into a stock solution (1 mM) of **Eu(*o*-OH)** and **Eu(*p*-OH)** in acetonitrile and drying with a stream of N_2 flow. The luminescent probe-loaded paper strips were hung from the top of a tall glass vial in the presence of various organophosphate (OP) vapors of various concentrations for various times, interferents, or other testing conditions. The luminescence was captured digitally under a UV lamp (365 nm).

Conclusions

We synthesized two red light-emitting luminescent probes, *viz.* **Eu(*o*-OH)** and **Eu(*p*-OH),** motivated by the reactivity of the OP AChE inhibitors with the nucleophilic OH group of the serine residue at the active site of AChE. The probe **Eu(*o*-OH)** was structurally characterized, showing square-antiprismatic geometry and the presence of intramolecular hydrogen bonding of *o*-OH and N groups of ***o*-HPIP**. Both the probes exhibit selective and sensitive detection of the sarin (GB) nerve agent simulant DCP in solution. The **Eu(*o*-OH)** probe remains highly selective for DCP compared to **Eu(*p*-OH)**, suggesting reactivity differences of the –OH groups mediated by their position and H-bonding capability. However, the probe **Eu(*p*-OH)** was more sensitive towards DCP, showing 'turn-off' luminescence at a lower concentration of DCP. The limits of detection of the probes **Eu(*o*-OH)** (18 ppb) and **Eu(*p*-OH)** (10 ppb) are among the best reported for the detection of nerve agent simulants. We seriously attempted to evaluate the reaction mechanism between the Eu(III) probes and DCP by NMR spectroscopy and other optical titration analyses. We successfully structurally identified the thermodynamically stable coordination polymer **[Eu(DHP)$_3$]$_n$**, formed due to *in situ* hydrolysis of DCP, resulting in the formation of DHP (diethyl hydrogen phosphate) with a strong binding affinity to Eu(III). Real-time detection of the nerve agent simulant in the vapor phase on a solid-state filter paper strip immobilized with the probes was shown, indicating the on-site utility of our system. The highly responsive Eu(III) probes are highly selective and sensitive to minimal concentrations of DCP vapors. The strategy could be applied to develop a prototype rapid, solid-state sensitive detection platform for nerve gases by integrating the luminescence signal output with a suitable optical detector.

Conflicts of interest

There are no conflicts to declare.

Acknowledgements

We thank IIT Kanpur for infrastructure and the Science and Engineering Research Board (SERB) for financial assistance (EMR/2016/000521). Z. A. and U. Y. gratefully acknowledge the University Grants Commission (UGC) and the Ministry of Human Resource Development (MHRD) for the PhD research fellowships.

References

1 (*a*) J. B. Sullivan Jr, G. B. Krieger and R. J. Thomas, Hazardous materials toxicology: clinical principles of environmental health, *J. Occ. Environ. Med.*, 1992, **34**, 365–371; (*b*) T. Urabe, K. Takahashi, M. Kitagawa, T. Sato, T. Kondo, S. Enomoto, M. Kidera and Y. Seto, Development of portable mass spectrometer with electron cyclotron resonance ion source for detection of chemical warfare agents in air, *Spectrochim. Acta, Part A*, 2014, **120**, 437–444; (*c*) S. Costanzi, J. H. Machado and M. Mitchell, Nerve agents: What they are, how they work, how to counter them, *ACS Chem. Neurosci.*, 2018, **9**, 873–885.

2 F. R. Sidell and J. Borak, Chemical warfare agents: II. Nerve agents, *Ann. Emerg. Med.*, 1992, **21**, 865–871.

3 (*a*) S. Fan, G. Zhang, G. H. Dennison, N. FitzGerald, P. L. Burn, I. R. Gentle and P. E. Shaw, Challenges in fluorescence detection of chemical warfare agent vapors using solid-state films, *Adv. Mater.*, 2020, **32**, 1905785; (*b*) S. Bencic-Nagale, T. Sternfeld and D. R. Walt, Microbead chemical switches: an approach to detection of reactive organophosphate chemical warfare agent vapors, *J. Am. Chem. Soc.*, 2006, **128**, 5041–5048.

4 (*a*) V. Kumar and M. P. Kaushik, Rapid and highly selective chromogenic detection of nerve agents with a cleft-shaped host, *Analyst*, 2011, **136**, 5151–5156; (*b*) V. Kumar and H. Rana, Chromogenic and fluorogenic detection and discrimination of nerve agents Tabun and VX, *Chem. Commun.*, 2015, **51**, 16490–16493.

5 L. Hedstrom, Serine protease mechanism and specificity, *Chem. Rev.*, 2002, **102**, 4501–4524.

6 (*a*) K. Kim, O. G. Tsay, D. A. Atwood and D. G. Churchill, Destruction and detection of chemical warfare agents, *Chem. Rev.*, 2011, **111**, 5345–5403; (*b*) N. Munro, Toxicity of the organophosphate chemical warfare agents GA, GB, and VX: Implications for public protection, *Environ. Health Perspect.*, 1994, **102**, 18–37; (*c*) D. Ajamai and J. Rebek, Jr., Chemical approaches for detection and destruction of nerve agents, *J. Org. Biomol. Chem.*, 2013, **11**, 3936–3942.

7 *The Pharmacological Basis of Therapeutics*, ed. J. G. Hardman, L. E. Limbird, P. B. Molinoff and R. W. Ruddon, McGraw-Hill, New York, 9th edn, 1995.

8 J. Misik, R. Pavlikova, J. Cabal and K. Kuca, Acute toxicity of some nerve agents and pesticides in rats, *Drug Chem. Toxicol.*, 2015, **38**, 32–36.

9 V. Kumar, G. Raviraju, H. Rana, V. K. Rao and A. K. Gupta, Highly selective and sensitive chromogenic detection of nerve agents (sarin, tabun and VX): a multianalyte detection approach, *Chem. Commun.*, 2017, **53**, 12954–12957.

10 H. H. Hill and S. J. Martin, Conventional analytical methods for chemical warfare agents, *Pure Appl. Chem.*, 2002, **74**, 2281–2291.

11 S. Royo, R. Martínez-Máñez, F. Sancenón, A. M. Costero, M. Parra and S. Gil, Chromogenic and fluorogenic reagents for chemical warfare nerve agents' detection, *Chem. Commun.*, 2007, 4839–4847.

12 (*a*) H. Sohn, S. Letant, M. J. Sailor and W. C. Trogler, Detection of fluorophosphonate chemical warfare agents by catalytic hydrolysis with a porous silicon interferometer, *J. Am. Chem. Soc.*, 2000, **122**, 5399–5400; (*b*) Y. S. Lu, S. Vijayakumar, A. Chaix, B. R. Pimentel, K. C. Bentz, S. Li, A. Chan, C. Wahl, J. S. Ha, D. E. Hunka and G. R. Boss, Remote detection of HCN, HF, and nerve agent vapors based on self-referencing, dye-impregnated porous silicon photonic crystals, *ACS Sens.*, 2021, **6**, 418–428.

13 M. A. K. Khan, Y. T. Long, G. Schatte and H. B. Kraatz, Surface studies of aminoferrocene derivatives on gold: electrochemical sensors for chemical warfare agents, *Anal. Chem.*, 2007, **79**, 2877–2884.

14 D. Williams and G. Pappas, Rapid identification of nerve agents Sarin (GB) and Soman (GD) with the use of a field-portable GC/SAW vapor detector and liquid desorption front-end device, *Field Anal. Chem. Technol.*, 1999, **3**, 45–53.

15 E. Steiner, S. J. Klopsch, W. A. English, B. H. Clowers and H. H. Hill, Detection of a chemical warfare agent simulant in various aerosol matrixes by ion mobility time-of-flight mass spectrometry, *Anal. Chem.*, 2005, **77**, 4792–4799.

16 N. R. Brletich, M. J. Waters, G. W. Bowen and M. F. Tracy, *Worldwide Chemical Detection Equipment Handbook*, Chemical and Biological Defense Information Analysis Center, Maryland, 1995.

17 Y. Sun and K. Y. Ong, *Detection Technologies for Chemical Warfare Agents and Toxic Vapors*, CRC Press, Washington DC, 2005.

18 B. Díaz de Greñu, D. Moreno, T. Torroba, A. Berg, J. Gunnars, T. Nilsson, R. Nyman, M. Persson, J. Pettersson, I. Eklind and P. Wästerby, Fluorescent discrimination between traces of chemical warfare agents and their mimics, *J. Am. Chem. Soc.*, 2014, **136**, 4125–4128.

19 (*a*) T. I. Kim, S. B. Maity, J. Bouffard and Y. Kim, Molecular rotors for the detection of chemical warfare agent simulants, *Anal. Chem.*, 2016, **88**, 9259–9263; (*b*) K. A. Van Houten, D. C. Heath and R. S. Pilato, Rapid luminescent detection of phosphate esters in solution and the gas phase using (dppe) Pt $\{S_2C_2$(2-pyridyl)$(CH_2CH_2OH)\}$, *J. Am. Chem. Soc.*, 1998, **120**, 12359–12360; (*c*) S.-W. Zhang and T. M. Swger, Fluorescent detection of chemical warfare agents: functional group specific ratiometric chemosensors, *J. Am. Chem. Soc.*, 2003, **125**, 3420–3421.

20 L. Chen, D. Wu and J. Yoon, Recent advances in the development of chromophore-based chemosensors for nerve agents and phosgene, *ACS Sens.*, 2017, **3**, 27–43.

21 Y. C. Cai, C. Li and Q. H. Song, Selective and visual detection of a nerve agent mimic by phosphorylation and protonation of quinolin oximes, *J. Mater. Chem. C*, 2017, **5**, 7337–7343.

22 L. Zeng, H. Zeng, L. Jiang, S. Wang, J. T. Hou and J. Yoon, A single fluorescent chemosensor for simultaneous discriminative detection of gaseous phosgene and a nerve agent mimic, *Anal. Chem.*, 2019, **91**, 12070–12076.

23 Y.-C. Cai and Q.-H. Song, Fluorescent chemosensors with varying degrees of intramolecular charge transfer for detection of a nerve agent mimic in solutions and in vapor, *ACS Sens.*, 2017, **2**, 834–841.

24 S. K. Sheet, B. Sen and S. Khatua, Organoiridium(III) complexes as luminescence color switching probes for selective detection of nerve agent simulant in solution and vapor phase, *Inorg. Chem.*, 2019, **58**, 3635–3645.

25 S. Khatua, B. Sen, M. Rabha, S. K. Sheet, D. Koner and N. Saha, Bis-heteroleptic Ru(II) polypyridine complex-based luminescent probes for nerve agent simulant and organophosphate pesticide, *Inorg. Chem. Front.*, 2020, **8**, 669–683.

26 R. Zhu, J. M. Azzarelli and T. M. Swager, Wireless hazard badges to detect nerve-agent simulants, *Angew. Chem., Int. Ed.*, 2016, **55**, 9662–9666.

27 (*a*) J.-C. G. Bünzli and C. Piguet, Taking advantage of luminescent lanthanide ions, *Chem. Soc. Rev.*, 2005, **34**, 1048–1077; (*b*) J.-C. G. Bünzli, Lanthanide luminescence for biomedical analyses and imaging, *Chem. Rev.*, 2010, **110**, 2729–2755.

28 M. C. Heffern, L. M. Matosziuk and T. J. Meade, Lanthanide probes for bioresponsive imaging, *Chem. Rev.*, 2014, **114**, 4496–4539.

29 A. J. Metherell, C. Curty, A. Zaugg, S. T. Saad, G. H. Dennison and M. D. Ward, Converting an intensity-based sensor to a ratiometric sensor: luminescence colour switching of an Ir/Eu dyad upon binding of a V-series chemical warfare agent simulant, *J. Mater. Chem. C*, 2016, **4**, 9664–9668.

30 H. Zhang, H. U. A. Xiufu, T. U. O. Xinlin, C. H. E. N. Chuanzhi and W. A. N. G. Xiaogong, Polystyrene microsphere-based lanthanide luminescent chemosensor for detection of organophosphate pesticides, *J. Rare Earths*, 2012, **30**, 1203–1207.

31 R. Shunmugam and G. N. Tew, Terpyridine–lanthanide complexes respond to fluorophosphate containing nerve gas G-agent surrogates, *Chem. – Eur. J.*, 2008, **14**, 5409–5412.
32 K. Gupta and A. K. Patra, Luminescent europium(III) ''Turn-On'' sensor for G-series chemical warfare simulants: A mechanistic investigation, *ACS Sens.*, 2020, **5**, 1268–1272.
33 M. De Sousa, B. De Castro, S. Abad, M. A. Miranda and U. Pischel, A molecular tool kit for the variable design of logic operations (NOR, INH, EnNOR), *Chem. Commun.*, 2006, 2051–2053.
34 G. H. Dennison, M. R. Sambrook and M. R. Johnston, VX and VG chemical warfare agents bidentate complexation with lanthanide ions, *Chem. Commun.*, 2014, **50**, 195–197.
35 (*a*) G. H. Dennison and M. R. Johnston, Mechanistic insights into the luminescent sensing of organophosphorus chemical warfare agents and simulants using trivalent lanthanide complexes, *Chem. – Eur. J.*, 2015, **21**, 6328–6338; (*b*) G. H. Dennison, C. G. Bochet, C. Curty, J. Ducry, D. J. Nielsen, M. R. Sambrook, A. Zaugg and M. R. Johnston, Supramolecular agent – simulant correlations for the luminescence based detection of V-series chemical warfare agents with trivalent lanthanide complexes, *Eur. J. Inorg. Chem.*, 2016, 1348–1358.
36 K. Skonieczny, A. I. Ciuciu, E. M. Nichols, V. Hugues, M. Blanchard-Desce, L. Flamigni and D. T. Gryko, Bright emission tunable fluorescent dyes based on imidazole and π-expanded imidazole, *J. Mater. Chem.*, 2012, **22**, 20649–20664.
37 M. A. Shipman, K. J. Ramhit and B. A. Blight, Sensing a Bacillis anthracis biomarker with well-known OLED emitter $EuTTA_3Phen$, *J. Mater. Chem. B*, 2016, **4**, 3043–3045.
38 (*a*) Q. Zhao, S. Liu, M. Shi, F. Li, H. Jing, T. Yi and C. Huang, Tuning photophysical and electrochemical properties of cationic iridium(III) complex salts with imidazolyl substituents by proton and anions, *Organometallics*, 2007, **26**, 5922–5930; (*b*) S. De, R. S. Kumar, A. Gauthaman, S. A. Kumar, P. Paira, A. Moorthy and S. Banerjee, Luminescent ruthenium(II)-*para*-cymene complexes of aryl substituted imidazo-1,10-phenanthroline as anticancer agents and the effect of remote substituents on cytotoxic activities, *Inorg. Chim. Acta*, 2021, **515**, 120066.
39 (*a*) S. Dasari, S. Singh, S. Sivakumar and A. K. Patra, Dual-sensitized luminescent europium(III) and terbium(III) complexes as bioimaging and light-responsive therapeutic agents, *Chem. – Eur. J.*, 2016, **22**, 17387–17396; (*b*) Z. Abbas, S. Dasari and A. K. Patra, Ternary Eu(III) and Tb(III) β-diketonate complexes containing chalcones: Photophysical studies and biological outlook, *RSC Adv.*, 2017, **7**, 44272–44281; (*c*) Z. Abbas, S. Dasari, M. J. Beltrán-Leiva, P. Cantero-López, D. Páez-Hernández, R. Arratia-Pérez, R. J. Butcher and A. K. Patra, Luminescent europium(III) and terbium(III) complexes of β-diketonate and substituted terpyridine ligands: Synthesis, crystal structures and elucidation of energy transfer pathways, *New J. Chem.*, 2019, **43**, 15139–15152.
40 K. Binnemans, Interpretation of europium(III) spectra, *Coord. Chem. Rev.*, 2015, **295**, 1–45.
41 S. I. Klink, G. A. Hebbink, L. Grave, P. G. Oude Alink, F. C. Van Veggel and M. H. Werts, Synergistic complexation of Eu^{3+} by a polydentate ligand and a bidentate antenna to obtain ternary complexes with high luminescence quantum yields, *J. Phys. Chem. A*, 2002, **106**, 3681–3689.
42 W. S. Lo, W. M. Kwok, G. L. Law, C. T. Yeung, C. T. L. Chan, H. L. Yeung, H. K. Kong, C. H. Cheng, M. B. Murphy, K. L. Wong and W. T. Wong, Impressive europium red emission induced by two-photon excitation for biological applications, *Inorg. Chem.*, 2011, **50**, 5309–5311.
43 J. Sun, B. Song, Z. Ye and J. Yuan, Mitochondria targetable time-gated luminescence probe for singlet oxygen based on a β-diketonate–europium complex, *Inorg. Chem.*, 2015, **54**, 11660–11668.
44 K. Gupta and A. K. Patra, A luminescent pH-responsive ternary europium(III) complex of β-diketonates and terpyridine derivatives as sensitizing antennae-photophysical aspects, anion sensing, and biological interactions, *Eur. J. Inorg. Chem.*, 2018, 1882–1890.
45 (*a*) W. D. Horrocks Jr. and D. R. Sudnick, Lanthanide ion probes of structure in biology. Laser-induced luminescence decay constants provide a direct measure of the number of metal-coordinated water molecules, *J. Am. Chem. Soc.*, 1979, **101**, 334–340; (*b*) A. Beeby, I. M. Clarkson, R. S. Dickins, S. Faulkner, D. Parker, L. Royle, A. S. De Sousa, J. A. G. Williams and M. Woods, Non-radiative deactivation of the excited states of europium, terbium and ytterbium complexes by proximate energy-matched OH, NH and CH oscillators: an improved luminescence method for establishing solution hydration states, *J. Chem. Soc., Perkin Trans. 2*, 1999, 493–504.
46 T. J. Dale and J. Rebek, Fluorescent sensors for organophosphorus nerve agent mimics, *J. Am. Chem. Soc.*, 2006, **128**, 4500–4501.
47 G. H. Dennison, M. R. Sambrook and M. R. Johnston, Interactions of the G-series organophosphorus chemical warfare agent sarin and various simulants with luminescent lanthanide complexes, *RSC Adv.*, 2014, **4**, 55524–55528.
48 D. Knapton, M. Burnworth, S. J. Rowan and C. Weder, Fluorescent organometallic sensors for the detection of chemical-warfare-agent mimics, *Angew. Chem., Int. Ed.*, 2006, **45**, 5825–5829.
49 S. Sarkar, A. Mondal, A. K. Tiwari and R. Shunmugam, Unique emission from norbornene derived terpyridine—A selective chemodosimeter for G-type nerve agent surrogates, *Chem. Commun.*, 2012, **48**, 4223–4225.
50 Y.-C. Cai, C. Li and Q.-H. Song, Fluorescent chemosensors with varying degrees of intramolecular charge transfer for detection of a nerve agent mimic in solutions and in vapor, *ACS Sens.*, 2017, **2**, 834–841.
51 J. Yao, Y. Fu, W. Xu, T. Fan, Y. Gao, Q. He, D. Zhu, H. Cao and J. Cheng, Concise and efficient fluorescent probe *via* an intromolecular charge transfer for the chemical warfare agent mimic diethylchlorophosphate vapor detection, *Anal. Chem.*, 2016, **88**, 2497–2501.
52 S. L. Huang, Y. L. Wu, F. Zeng, L. H. Sun and S. Z. Wu, Handy ratiometric detection of gaseous nerve agents with

AIE-fluorophore-based solid test strips, *J. Mater. Chem. C*, 2016, **4**, 10105.

53 L. Chen, D. Wu and J. Yoon, Recent advances in the development of chromophore-based chemosensors for nerve agents and phosgene, *ACS Sens.*, 2018, **3**, 27–43.

54 M. L. Aulsebrook, B. Graham, M. R. Grace and K. L. Tuck, Lanthanide complexes for luminescence-based sensing of low molecular weight analytes, *Coord. Chem. Rev.*, 2018, **375**, 191–220.

55 A. Barba-Bon, A. M. Costero, S. Gil, F. Sancenón and R. Martínez-Máñez, Chromo-fluorogenic BODIPY-complexes for selective detection of V-type nerve agent surrogates, *Chem. Commun.*, 2014, **50**, 13289–13291.

56 G.-L. Law, K.-L. Wong, X. Zhou, W.-T. Wong and P. A. Tanner, *Inorg. Chem.*, 2014, **50**, 13289–13291.

57 (*a*) K. Tuovinen, Organophosphate-induced convulsions and prevention of neuropathological damages, *Toxicology*, 2004, **196**, 31–39; (*b*) T. C. Marrs, Organophosphate poisoning, *Pharmacol. Ther.*, 1993, **58**, 51–66.

58 *SMART & SAINT Software Reference manuals, Version 6.45*, Bruker Analytical X-ray Systems, Inc., Madison, WI, 2003.

59 G. M. Sheldrick, *SADABS, Software for empirical absorption correction, Ver. 2.05*, University of Göttingen, Göttingen, Germany, 2002.

60 *SHELXTL Reference Manual, Ver. 6.1*, Bruker Analytical X-ray Systems, Inc., Madison, WI, 2000.

61 G. M. Sheldrick, *SHELXTL, Ver. 6.12*, Bruker AXS Inc., WI, Madison, 2001.

62 G. M. Sheldrick, Crystal structure refinement with SHELXL, *Acta Crystallogr., Sect. C: Struct. Chem.*, 2015, **71**, 3–8.

63 O. V. Dolomanov, L. J. Bourhis, R. J. Gildea, J. A. K. Howard and H. Puschmann, OLEX2: a complete structure solution, refinement and analysis program, *J. Appl. Crystallogr.*, 2009, **42**, 339–341.